
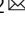



Isoelectronic aluminum-doped gallium nitride alpha-voltaic cell with efficiency exceeding 4.5%

Runlong Gao^{1,2}, Linyue Liu²  , Xiaochuan Xia³, Pengying Wan⁴, Xiao Ouyang⁵, Wuying Ma², Xinlei Geng³, Hongyun Wang³, Ruiliang Xu³, Kexiong Zhang³, Hongwei Liang³ & Xiaoping Ouyang² 

Although alpha-voltaic cells have shown great potential in unattended miniaturized systems for compact, long-lifetime and independence of external energy input, the power conversion efficiency of state-of-the-art alpha-voltaic cells is still much lower than the theoretical limit. Here, an alpha-voltaic cell based on a gallium nitride transducer with PIN structure is designed and investigated. We find that isoelectronic aluminum-doping is an effective way for boosting the performance of the gallium nitride transducer by decreasing the unintentional doping concentration, deep trap concentration, and dislocation density in the gallium nitride epilayer. The isoelectronic aluminum-doped cell demonstrates a large depletion region of 1.89 μm and a charge collection efficiency of 61.6% at 0 V bias, resulting in a high power conversion efficiency of 4.51%, comparable to the best gallium nitride beta-voltaic cells. This work increases alpha-voltaic cell efficiency, bridging the gap between nuclear micro-batteries and real applications in extreme environments.

¹Sino-French Institute of Nuclear Engineering and Technology, Sun Yat-Sen University, Zhuhai, China. ²State Key Laboratory of Intense Pulsed Radiation Simulation and Effect, Northwest Institute of Nuclear Technology, Xi'an, China. ³School of Microelectronics, Dalian University of Technology, Dalian, China. ⁴School of Microelectronics, Xi'an Jiaotong University, Xi'an, China. ⁵Key Laboratory of Beam Technology of Ministry of Education, College of Nuclear Science and Technology, Beijing Normal University, Beijing, China. email: liulinyue@nint.ac.cn; oyxp2003@aliyun.com

Radio-voltaic cell is a kind of nuclear micro-battery, directly converting ionizing radiations (alpha, beta or gamma) emitted by long-life radioisotopes into electric energy using semiconductor transducers (Fig. 1a)^{1,2}. RV cells can provide ultra-stable output power for decades in extreme environments without any maintenance or external energy replenishment (Fig. 1b)³, which are expected to play a significant role in spacecrafts, intelligent weapons, deep-sea probes, implantable chips and other unique applications (Fig. 1c), where commonly used batteries cannot be employed independently^{4–6}.

In general, radio-voltaic cell tends to use low energy β -sources (^3H and ^{63}Ni , etc.) with low ionization-induced damage to transducers for realizing long service life. However, there are some technical limitations for beta-voltaic cells, such as the upper limit of power density being low and power conversion efficiency (PCE) decreasing significantly with the increase in activity of β -source due to its self-absorption effect^{7–9}. In contrast with β -sources, α -sources, e.g., ^{238}Pu and ^{241}Am , possess much higher energy and ionization density in the transducers, indicating that alpha-voltaic (AV) cells are expected to break through the technical bottleneck of beta-voltaic cells for achieving higher power density and PCE simultaneously^{10,11}. One of the main challenges in the development of AV cells is the radiation tolerance of transducers because the radiation damage caused by α -particles to semiconductors is much more severe than β -particles^{12,13}. Limited by the insufficient radiation tolerance of most of the mature traditional semiconductors^{14,15}, Si, Ge and GaAs cannot maintain the long-term stable operation of AV cells. Thus, transducers based on wide bandgap semiconductors with ultrahigh radiation tolerance and excellent stability under harsh environments are being actively pursued^{16–19}. At present, silicon carbide (SiC) and diamond transducers with PN junction, Schottky junction and PIN junction have been fabricated and used for several AV cell prototypes^{11,20,21}. Our recent study reported a high-performance

AV cell based on a SiC PIN junction transducer²², exhibiting a high open-circuit voltage (V_{OC}) of 1.99 V and a remarkable power conversion efficiency (PCE) of 0.88%, which is 8 times higher than the previously reported SiC AV cells. Theoretically, diamond is undoubtedly the most ideal transducer material because it exhibits an outstanding radiation tolerance²³ and maximum possible PCE^{1,7,24}. The high-power density AV cell based on 130 vertical diamond Schottky transducers, which are serially connected with a total area of 15 cm², is investigated by Bormashov et al., rendering a maximum power density (P_{max}) of 2.4 $\mu\text{W cm}^{-2}$, V_{OC} of 1.85 V and a considerable PCE of 3.6% using high-activity ^{238}Pu α -source, which is the highest reported PCE of AV cells¹³. Liu et al. have reported an effective way to improve V_{OC} and PCE of diamond Schottky AV cells by deploying a zinc oxide (ZnO) film as the electron transport layer (ETL) to reduce the recombination rate of minority carriers²⁵, V_{OC} of 1.43 V and PCE of 1.42% were attained under the irradiation of a low-activity ^{241}Am α -source consequently. With the rapid improvement of gallium nitride (GaN) technology (Fig. 1d)^{26–28}, GaN is also being considered as a valuable transducer material for RV cells because of its large displacement energy (45 eV for Ga and 109 eV for N), high stopping power for α -particles and excellent electrical properties^{29,30}, which is expected to achieve a strong radiation tolerance and superior output performance (V_{OC} , P_{max} and PCE)^{31,32}. Furthermore, the price of GaN transducers on heteroepitaxial substrates is significantly lower than the electronic-grade single-crystal diamond^{33–35}. In recent years, GaN beta-voltaic cells have been widely investigated by several research groups, attaining valuable experimental and theoretical results^{5,36–42}. However, GaN AV cells have not been reported yet, as well as the quantitative evaluation of service life is still unclear.

In this study, a GaN AV cell, with a PIN junction, is fabricated and its electrical performance is verified using an He-ion

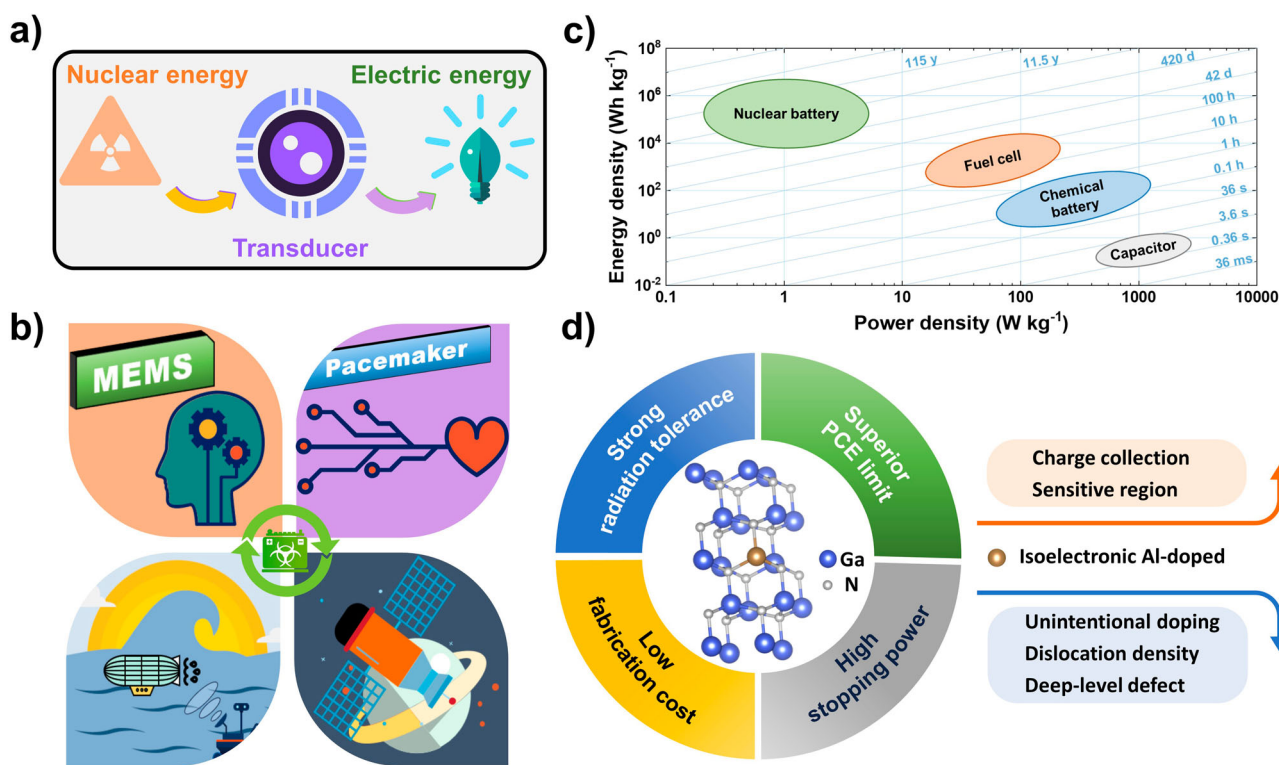


Fig. 1 Concept, characteristics and applications of efficient nuclear micro-battery. **a** Schematic depiction of nuclear micro-battery and its application in **b** micro-electromechanical systems (MEMS), cardiac pacemaker, deep-sea sonar and spacecraft. **c** Simplified Ragone plot of several electrical energy storage (EES) systems. **d** Significant properties of GaN semiconductor material with isoelectronic Al-doping.

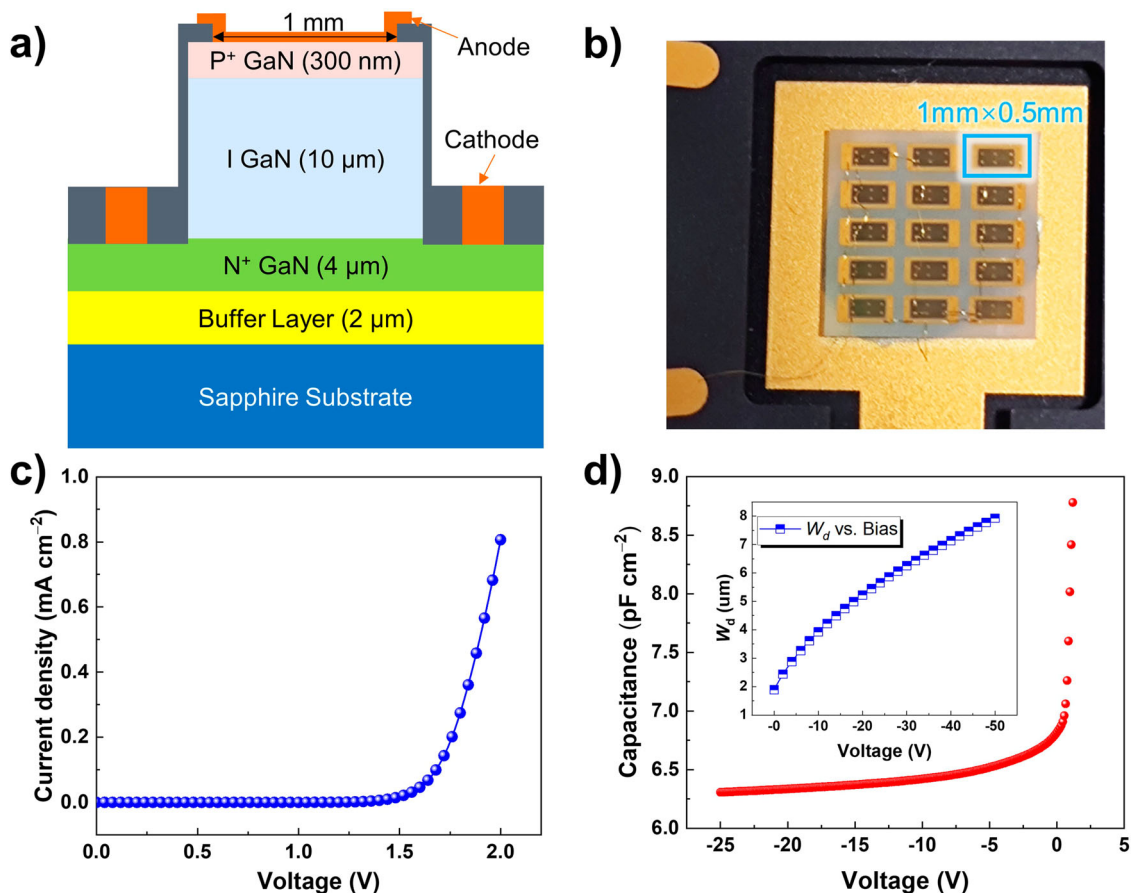


Fig. 2 Structure and electronic characteristics of GaN transducer. **a** Schematic drawing of the PIN structure of GaN transducer. **b** Digital photograph of the front-view of GaN transducer array. **c** Forward I - V and **d** reverse C - V curves of GaN transducer at room temperature without irradiation.

electrostatic accelerator, serving as an α -source. Then, isoelectronic Al-doping is carried out to reduce unintentional doping concentration, dislocation density and deep-level defect in the epilayer of GaN transducer, improving the width and charge collection efficiency of the sensitive region of GaN transducer. In addition, the performance degradation of GaN transducers under He ions irradiation is systematically studied for evaluating the lifetime of GaN AV cells.

Results and discussion

Design and characteristics of GaN transducer. Figure 2a shows the structure of GaN transducer. The epitaxial layers of GaN transducer are grown on a sapphire substrate (2 inch) by the metal-organic chemical vapor deposition (MOCVD) method. There are multiple layers from the bottom to top: n^+ -GaN layer (4 μm in thickness, doped with Si atoms ($5 \times 10^{18} \text{ cm}^{-3}$)), i -GaN layer (10 μm in thickness, doped with isoelectronic Al atoms) and p^+ -GaN layer (0.3 μm in thickness, doped with Mg atoms ($1 \times 10^{19} \text{ cm}^{-3}$)). Note that the concentration of isoelectronic Al-doping in the i -GaN layer is 0.214%, as confirmed by secondary ion mass spectroscopy (SIMS). Compared with the as-grown GaN layer, the advantage of isoelectronic Al doping at the given level is proved to have an obvious effect on improving crystalline quality and electrical properties of GaN transducer (for the advantage of isoelectronic Al doping in the i -GaN layer see Supplementary Note 1)⁴³. Then, the wafer was cut into small pieces. After a series of processes, a Ni/Au (20 nm/20 nm) ohmic contact electrode was formed on the p^+ -GaN layer as an anode and a Ti/Al/Ni/Au stack was deposited for ohmic contact on the n^+ -GaN layer as a cathode. On the

anode, patterned SiO_2 and Cr/Au layers acted as the passivation layer and field plate, respectively. Finally, the gold wire bonding method was used to electrically connect the GaN unit. Figure 2b presents a photograph of the front view of GaN transducer array with an overall active area of 7.5 mm^2 , consisting of 15 single GaN transducers.

Electronic characteristics of GaN transducer were analyzed by forward current–voltage (I - V) and capacitance–voltage (C - V) characteristics measurement respectively (Fig. 2c, d). Moreover, GaN exhibits typical diode rectifying characteristics with the value of forward threshold voltage is ~ 1.6 V. Also, the donor concentration of i -GaN ($N_d = 8.30 \times 10^{14} \text{ cm}^{-3}$) can be extracted from the relationship between $1/C^2$ and V , which can be expressed by Eq. (1):

$$\frac{1}{C^2} = \frac{2(-V + V_{bi} - 2kT/q)}{q\epsilon_r\epsilon_0 N_d} \quad (1)$$

where V_{bi} is the built-in potential of GaN transducer (~ 3.0 V), k refers to the Boltzmann constant ($1.38 \times 10^{-23} \text{ J K}^{-1}$), T represents the room temperature (300 K), q denotes the electron charge ($1.60 \times 10^{-19} \text{ C}$), ϵ_r is the relative dielectric constant (8.9) for GaN and ϵ_0 is the permittivity of free space ($8.85 \times 10^{-14} \text{ F cm}^{-1}$). The inset in Fig. 2d shows the depletion region width (W_d) of GaN transducer at a low reverse bias, which can reach up to 1.89 μm at 0 V. According to the ideal pin diode model, the width of the depletion layer is inversely proportional to the electron concentration in the i -GaN layer. The lower electron concentration of i -GaN layer is crucial for expanding the width of depletion layer. The background electron concentration of undoped i -GaN grown by MOCVD is always influenced by the

unintentionally impurities, such as oxygen (O), silicon (Si) and carbon (C). Si and O will substitute on the Ga and N sites, respectively, and usually act as donor in i-GaN layer. In particular, C plays a dual role in i-GaN layer, which can behave as a shallow donor if it occupies the site of Ga, or a deep acceptor if it occupies the site of N⁴⁴. For the undoped i-GaN layer, the Si concentration is close to that of C, causing C tend to incorporate as C_N, and the electron concentration of i-GaN is equal to the sum of the concentration of Si and O minus that of C ($\sim 1 \times 10^{16} \text{ cm}^{-3}$). For the isoelectronic Al-doped i-GaN layer, since both Si and Al occupy the Ga site, Al will inhibit the doping of Si effectively, causing the C concentration exceeds that of Si in GaN. At this time, C will both substitute Ga and N sites with the number of C_{Ga} and C_N is close equal⁴⁵. Accordingly, the Al-doped i-GaN exhibits semi-insulating properties with the electron concentration could be at least an order of magnitude lower than that of undoped i-GaN. Hence, it is considered that the isoelectronic Al-doping is beneficial to realize large depletion region, which is helpful for the energy deposition of α -particles subsequently.

Energy transfer mechanism and simulation of GaN AV cell. As shown in Fig. 3a, the α -particles penetrate into the GaN transducer from its upper surface. In this case, electron-hole pairs are ionized in the sensitive region of GaN transducer by absorbing the energy of α -particles, then separate and drift to the electrodes under the effect of electric field and concentration gradient. The sensitive region is composed of two parts, i.e., depletion region and diffusion region. In the diffusion region, the minority carriers (holes) render a certain probability to diffuse into the depletion region and contribute to the current output, the diffusion region

width (L_d) can be expressed by Eq. (2)⁴⁶:

$$L_d = \sqrt{\frac{kT}{q} \mu \tau} \quad (2)$$

where μ is the mobility of holes ($10\text{--}30 \text{ cm}^2 \text{ V}^{-1} \text{ s}^{-1}$), and τ refers to the lifetime of holes ($\sim 1 \text{ ns}$). Therefore, one can estimate that the maximum value of L_d is about $0.28 \text{ }\mu\text{m}$, which is consistent with EBIC experimental results⁴⁷. As shown in Fig. 3b, the penetration depth of α -particles depending on the irradiation energies of 1 to 5.5 MeV in intrinsic GaN layer was calculated by the Stopping and Range of Ions in Matter (SRIM) software. Results indicate that the penetration depth of α -particles in intrinsic GaN layer increases exponentially as the irradiation energies increase, which is 6.69, 9.53, and $14.59 \text{ }\mu\text{m}$ corresponding to 3, 4 and 5.5 MeV, respectively. Figure 3c presents the Geant4 simulation on the dependence of the energy deposition in intrinsic GaN layer of a single α -particle (3, 4, 5, and 5.5 MeV) on the incident depth, which can be described by the Bethe formula⁴⁸. Furthermore, based on the model of GaN transducer, the energy deposition of α particles (E_{dep}) distributed in each layer of GaN transducer can be simulated by Geant4 software. Figure 3d shows less than a third of the α particle's energy deposited in the sensitive region (orange and green), and most of the contribution comes from the depletion region. As the energy of α particles decrease from 5.5 MeV to 3 MeV, E_{dep} increase significantly, which is about 0.65 MeV, 0.78 MeV, and 0.91 MeV, respectively. It indicates that reasonable selection of α -sources with lower energy is helpful for improving its energy deposition efficiency in sensitive region.

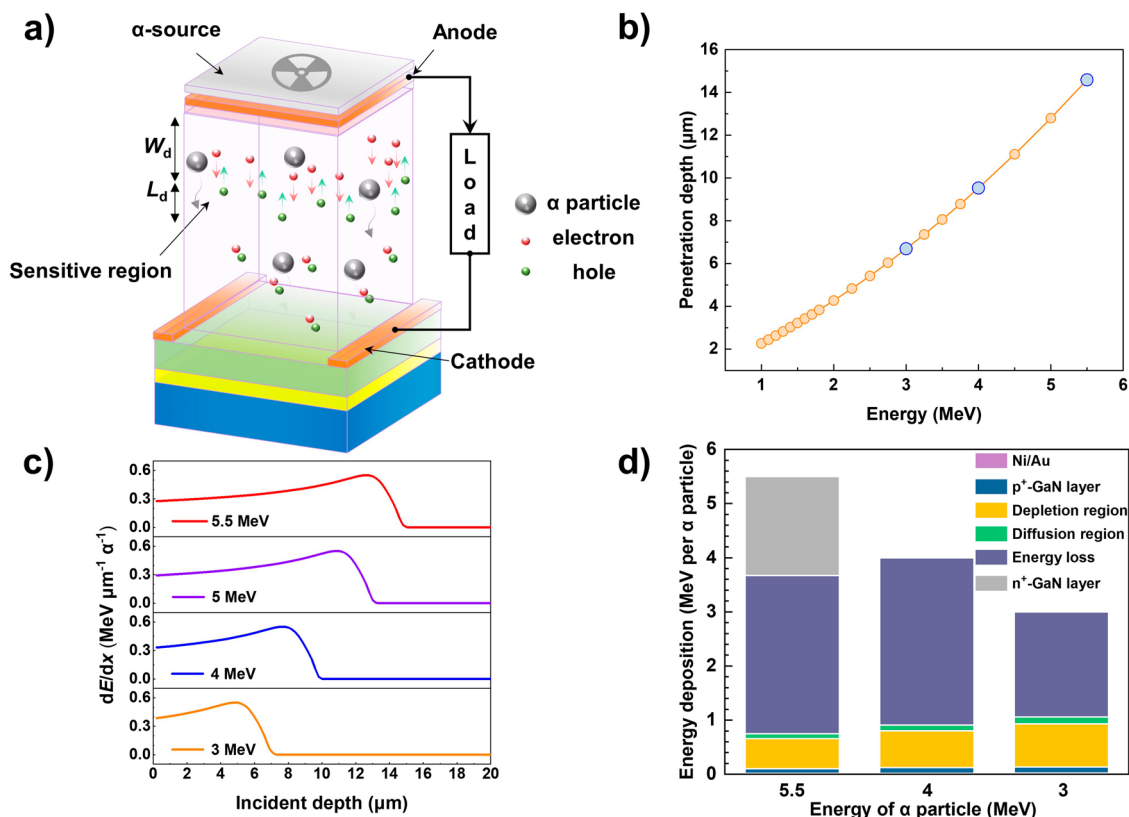


Fig. 3 Energy transfer mechanism of the GaN AV cell. **a** Schematic of the interaction process between α -particles and GaN transducer. **b** Penetration depth of α -particles in intrinsic GaN layer calculated by SRIM software. **c** Dependence of the α -particle's energy deposition in intrinsic GaN layer on the incident depth. **d** Energy deposition of α -particle (5.5 MeV, 4 MeV, and 3 MeV) in different regions of GaN transducer at 0 V bias.

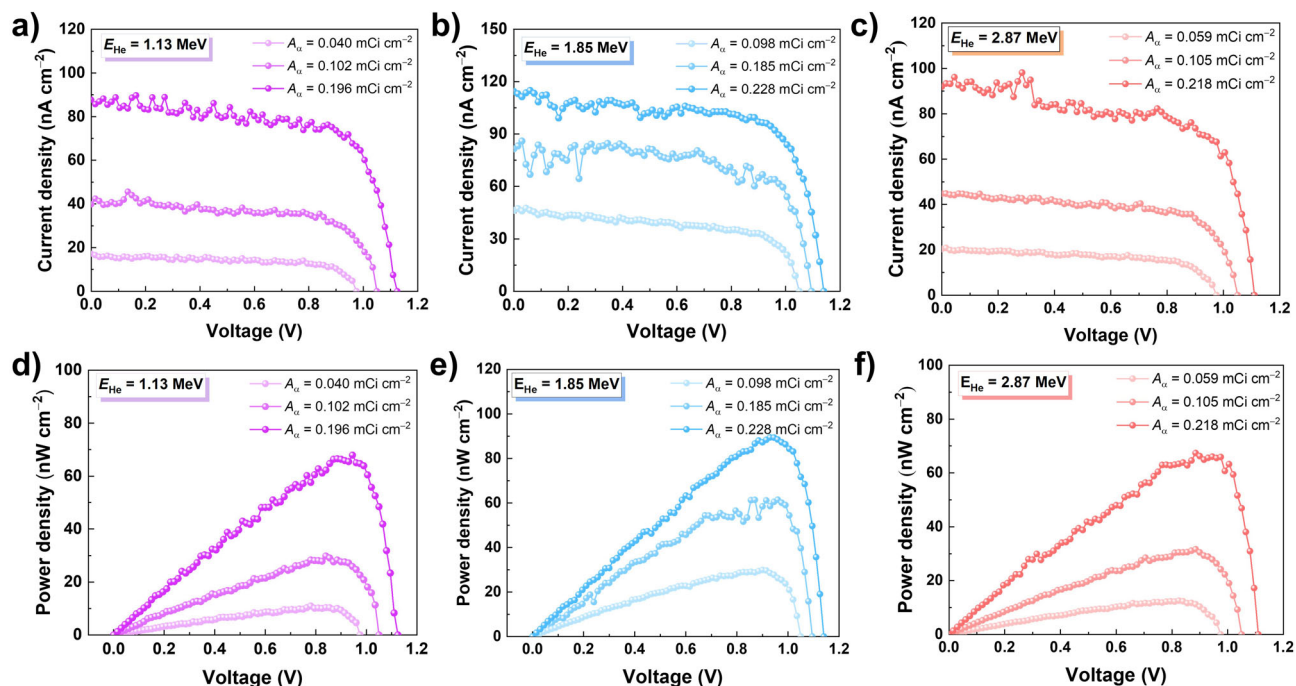


Fig. 4 Electrical characteristics of GaN AV cell. I - V curves of GaN AV cell at E_{He} of **a** 1.13 MeV, **b** 1.85 MeV and **c** 2.87 MeV with different A_{α} values; and P - V curves of GaN AV cell at E_{He} of **d** 1.13 MeV, **e** 1.85 MeV and **f** 2.87 MeV with different A_{α} values.

Charge collection efficiency of GaN transducer. Charge collection efficiency (η_{cce}) is the ratio of carriers' number collected by the GaN transducer to the quantity of carriers produced in the sensitive region, which is the key parameter for evaluating the performance of GaN transducers. Herein, an ORTEC spectroscopy system cooperate with a compound α -source (^{243}Am , $E_{\alpha} = 5.28$ MeV; ^{244}Cm , $E_{\alpha} = 5.80$ MeV) are used to measure the α -particle height spectra response and η_{cce} of the GaN transducer (for charge collection efficiency measurement see Supplementary Note 2). Therefore, the η_{cce} of GaN transducer can be obtained using Eq. (3):

$$\eta_{\text{cce}} = \frac{\omega_{\text{GaN}}}{\omega_{\text{Si}}} \cdot \frac{P_{\text{GaN}}}{P_{\text{Si}}} \cdot \frac{G_{\text{Si}}}{G_{\text{GaN}}} \cdot \frac{E_{\text{Si}}}{E_{\text{dep}}} \quad (3)$$

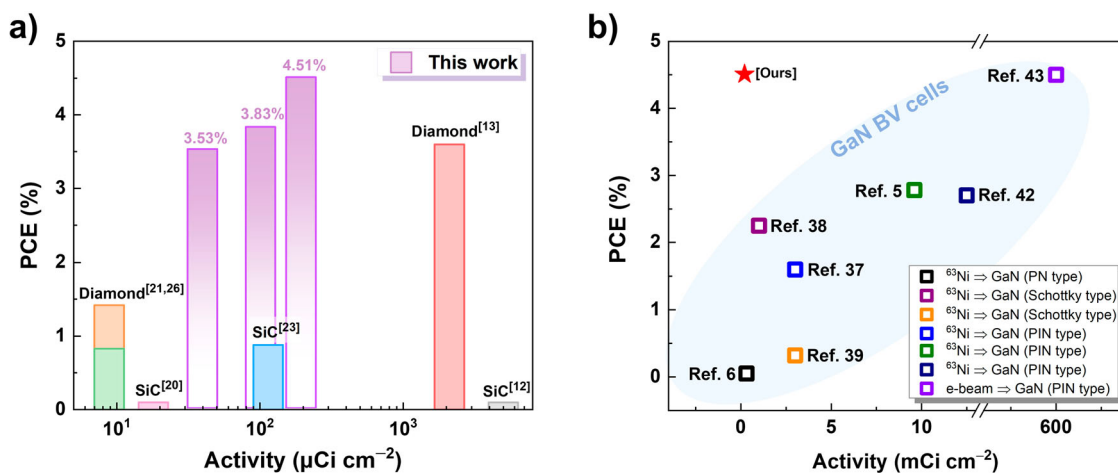
where ω_{GaN} (8.9 eV) and ω_{Si} (3.6 eV) represent the mean ionization energy of GaN and Si; P_{GaN} (134.22 at 0 V bias) and P_{Si} (732.60 for ^{243}Am) refer to the peak centroid channels of GaN transducer and Si detector (Supplementary Fig. 2b and 2c); G_{GaN} and G_{Si} denote the amplifier gains of GaN transducer (300) and Si detector (50); E_{dep} (0.65 MeV at 0 V bias) and E_{Si} (5.28 MeV for ^{243}Am) refer to the sensitive region's energy depositions of GaN transducer and Si detector, respectively. As a result, the η_{cce} of GaN transducer is up to 61.3% at 0 V bias, and raise greatly with the reverse bias increase from 0 V to 3 V (Supplementary Fig. 2d). Such a high η_{cce} value is advantageous for achieving high-efficiency AV cells, this can be attributed to the low dislocation densities (screw dislocation densities (SDDs), edge dislocation densities (EDDs) and total threading dislocation densities (TDDs)) and deep-level defects of i-GaN layer restrained by isoelectronic Al doping⁴⁹. Due to the higher bonding energy of the N-Al bond (2.88 eV) than that of the N-Ga bond (2.24 eV), Ga could be replaced by Al and introduce a local strain for restraining the propagation of the dislocation around the N-Al bond^{50,51}. Thus, the dislocation densities and deep level defects are reduced by isoelectronic Al doping, which can reduce the minority carrier recombination rate in the sensitive region of GaN transducer.

Electrical characteristics of GaN AV cell. Figure 4 illustrates the electrical output characteristics of the GaN AV cell under the irradiation of He ions accelerator used as the equivalent α -radioisotope sources (for detailed experimental conditions see Supplementary Note 3). Figure 4a-c display the I - V curves of GaN AV cell carried with different equivalent activity (A_{α}) of α -source at the energy of (E_{He}) 1.13 MeV, 1.85 MeV and 2.87 MeV, respectively. It is obvious that the output current is quite stable with an output voltage, ranging from 0 V to ~ 0.85 V, while it decreases exponentially as the output voltage increases from 0.85 V to V_{OC} (~ 1.10 V). Under the same E_{He} , e.g., 1.13 MeV (Fig. 4a), significant linear improvements in I_{SC} are observed when A_{α} increases from 0.040 to 0.196 mCi cm^{-2} , resulting in a slight increase in V_{OC} . Meanwhile, Fig. 4d-f show the P - V curves of GaN AV cell, corresponding to the E_{He} of 1.13 MeV, 1.85 MeV, and 2.87 MeV, respectively. When the output voltage of GaN AV cell increases from 0 V to ~ 0.85 V, the output power increases linearly to the P_{max} and, then, quickly decreases to zero at V_{OC} . The electrical parameters of GaN AV cell corresponding to the aforementioned electrical characteristic curves are extracted and summarized in Table 1. It indicates that the PCE of GaN AV cell at E_{He} of 1.13 MeV clearly surpasses the conditions of 1.85 MeV and 2.87 MeV, which can be ascribed to the better matching-degree between the sensitive region width of GaN transducer and E_{He} . It can be observed that the optimal PCE of 4.51% is achieved when the equivalent activity of α -source is 0.196 mCi cm^{-2} , where V_{OC} , I_{SC} , P_{max} and FF of GaN AV cell are found to be 1.13 V, 86.80 nA cm^{-2} , 67.91 nW cm^{-2} and 0.70, respectively.

It is worth noting that, the PCE of GaN AV cell in this work is the highest among all AV cells reported so far (Fig. 5a), which is mainly attributed to the significant improvement in sensitive region width and η_{cce} of GaN transducer. Figure 5b presents the PCE comparison with reported GaN RV cells with transducers based on the structure of Schottky, PN and PIN types. It is exciting that, the PCE of GaN AV cell in this work (red star) is comparable to the optimal GaN beta-voltaic cell (purple square), and the activity of radioisotope source required is four orders of magnitude less than that of GaN beta-voltaic cell

Table 1 Comparison of electrical characteristics of GaN AV cell with different E_{He} and B_i values.

E_{He} (MeV)	A_{α} (mCi cm $^{-2}$)	V_{OC} (V)	I_{SC} (nA cm $^{-2}$)	P_{max} (nW cm $^{-2}$)	PCE (%)	FF
1.13	0.040	0.98	16.44	10.92	3.53 ± 0.44	0.68
	0.102	1.05	41.20	30.00	3.83 ± 0.48	0.69
	0.196	1.13	86.80	67.91	4.51 ± 0.57	0.70
1.85	0.098	1.05	46.58	29.88	2.58 ± 0.32	0.61
	0.185	1.10	81.73	61.44	2.80 ± 0.35	0.68
	0.228	1.14	112.93	89.40	3.31 ± 0.42	0.69
2.87	0.059	0.98	20.36	12.54	1.20 ± 0.15	0.63
	0.105	1.05	44.62	31.62	1.69 ± 0.21	0.67
	0.218	1.11	92.84	67.38	1.74 ± 0.22	0.65

**Fig. 5 PCE comparison with the reported radio-voltaic cell. a** PCE of AV cells based on different semiconductor materials. **b** PCE comparison between GaN AV cell and GaN beta-voltaic cells based on various transducer structures.

(600 mCi cm^{-2}). This is because of the energy and ionization efficiency of α -radioisotopes are much higher than that of β -radioisotopes, indicating that AV cells are capable to save the weight of radioisotope sources, and expected to achieve smaller size and higher efficiency simultaneously.

Lifetime evaluation of GaN AV cell. Since α -particles lead to severe lattice damage to the sensitive region of GaN transducer and even destroy the device, a systematic study on the performance degradation of GaN transducer after He ions irradiation is quite important for evaluating the lifetime of GaN AV cells. Thus, a set of GaN transducers with excellent performance consistency was selected and irradiated by He-ions emitted from the accelerator with the energy of 1.5 MeV at room temperature. Five GaN transducers were exposed to different He ions irradiation fluences of 1×10^{10} to $3 \times 10^{15} \text{ cm}^{-2}$ (Fig. 6a) exhibits the α -particle height spectra response of GaN transducers before and after He-ions irradiation at a bias of 0 V, where the peak centroid channel of the fresh GaN transducer was initially at 140, no change occurred at the fluence of $1 \times 10^{10} \text{ cm}^{-2}$, shifted to 50.76 at a fluence of $5 \times 10^{12} \text{ cm}^{-2}$, and reached 24.92 at a fluence of $1 \times 10^{13} \text{ cm}^{-2}$. Finally, the α -particle height spectra could no longer be recorded as the He-ions irradiation fluences continued to increase. Figure 6b summarizes the η_{cvc} degradation of GaN transducer after continuous He-ions irradiation. We estimate the threshold fluence to disable (a quarter of initial value) a GaN transducer is about $1 \times 10^{13} \text{ cm}^{-2}$, which is comparable to the high-radiation-tolerance diamond transducer reported so far¹³, and then the service life of GaN AV cell is about 1500 h while carrying α -source with an activity of 0.05 mCi cm^{-2} . To prolong the lifetime

of GaN AV cells, on the one hand, it is necessary to improve the PCE of GaN AV cells for reducing the activity of α -source and, on the other hand, one needs to relieve the negative effect of radiation damage on the sensitive region of GaN transducer.

Conclusion

In summary, we explored and proposed high-efficiency AV cell based on GaN PIN transducer with an isoelectronic Al-doped epilayer. An ultrahigh PCE of 4.51% was achieved with an equivalent radioisotope activity of 0.196 mCi cm^{-2} , which is the highest among reported AV cells. The superior performance in GaN AV cell is mainly attributed to the isoelectronic Al-doping. On one hand, the unintentional doping concentration, deep trap concentration and dislocation density in GaN epilayer was decreased effectively. On the other hand, the width and charge collection efficiency of the sensitive region of GaN transducer was increased concomitantly. In addition, performance degradation of GaN transducer after He ions irradiation at different fluences (1×10^{10} to $3 \times 10^{15} \text{ cm}^{-2}$) has been systematically studied and the lifetime of GaN AV cell (1500 h) has been evaluated. In the future, the PCE and lifetime of GaN AV cell is expected to be further improved by optimizing the structure and technological process of GaN transducer. This work demonstrates an effective way for boosting the performance of GaN AV cells, which may promote the application of nuclear micro-batteries in extreme environments.

Methods

Preparation of GaN transducer. The GaN epitaxial layers with p-i-n structure were grown on sapphire substrate by metal-organic chemical vapor deposition (MOCVD). During the growth of the GaN epitaxial layers, TMGa (650 sccm,

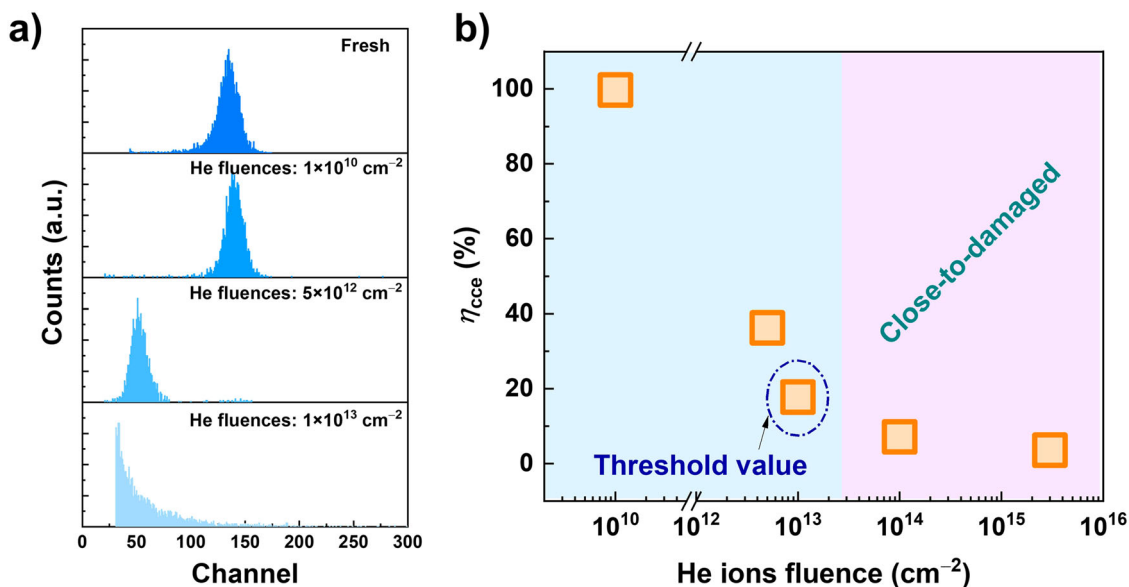


Fig. 6 Radiation tolerance assessment of GaN AV cell. **a** The variation of α -particle height spectra response of GaN transducers under He ions irradiation of different fluences of 1×10^{10} to $3 \times 10^{15} \text{ cm}^{-2}$. **b** η_{cce} degradation of GaN transducers after He ions irradiation.

1000 mbar) and NH_3 were used as Ga and N precursors, with a V/III ratio of about 520. First, 2 μm -thick unintentionally doped GaN buffer layer, was grown on sapphire substrate (0001). Then, 4 μm -thick GaN N⁺-layer, was grown on GaN buffer layer at 1100 °C. Silane (SiH_4 , 110 sccm, 1000 mbar) was used as Si source. Then, 10 μm -thick Al-doped GaN i-layer, was grown on GaN N⁺-layer at 1100 °C. Trimethylaluminum (TMAL, 25 sccm, 1000 mbar) was used as Al source. Then, 300 nm-thick GaN P⁺-layer, was grown on GaN i-layer at 1000 °C. Magnesium (MgCp₂, 300 sccm, 1000 mbar) was used as Mg source.

Then, the GaN epitaxial layers were cleaned by using acetone, isopropanol, and deionized water for 20 min. Then, the N⁺-GaN layer was exposed using inductively coupled plasma (ICP) dry etching with 11 μm etching depth. Then, the 1 μm SiO_2 passivation layer was deposited on the GaN using plasma-enhanced chemical vapor deposition (PECVD). After exposing the electrode region using buffered oxide etch (BOE) wet etching, Ni/Au multilayer was deposited as the anode and Ti/Al/Ni/Au multilayer was deposited as the cathode⁴³.

Electrical measurements. I–V and C–V characteristics of GaN transducer measurement were carried out using Keithley B1505A SCS at room temperature. Charge collection efficiency measurement of the GaN transducer was carried out by using an ORTEC spectroscopy system found in Supplementary Fig. 2. Electrical characteristics of the GaN AV cell under the irradiation of He ions were measured by using a Keysight B2902A Source/Measure Unit (SMU) found in Supplementary Fig. 3.

Data availability

The data that support the findings of this study are available from the corresponding author upon reasonable request.

Received: 10 January 2023; Accepted: 28 April 2023;

Published online: 04 July 2023

References

- Prelas, M. A. et al. A review of nuclear batteries. *Prog. Nucl. Energy* **75**, 117–148 (2014).
- Ayodele, O. L., Sanusi, K. O. & Kahn, M. T. Nuclear battery: a route of environmentally friendly energy. *J. Eng. Des. Technol.* **17**, 172–182 (2019).
- Wu, M. & Zhang, J. Design and simulation of high conversion efficiency betavoltaic battery based on a stacked multilayer structure. *AIP Adv.* **9**, 075124 (2019).
- Gao, H., Luo, S., Zhang, H., Wang, H. & Fu, Z. Demonstration, radiation tolerance and design on a betavoltaic micropower. *Energy* **51**, 116–122 (2013).
- Xi, S. et al. Researches on the performance of GaN-PIN betavoltaic nuclear battery. *Radiation Effects and Defects in Solids* **177**, 213–229 (2022).
- Aydin, S. & Kam, E. Investigation of nickel-63 radioisotope-powered GaN betavoltaic nuclear battery. *Int. J. Energy Res.* **43**, 8725–8738 (2019).
- Liu, Y. M., et al. A 4H-SiC betavoltaic battery based on a ⁶³Ni source. *Nucl. Sci. Techniques* **29**. <https://doi.org/10.1007/s41365-018-0494-x> (2018).
- Spencer, M. G., & Alam, T. High power direct energy conversion by nuclear batteries. *Appl. Phys. Rev.* **6**. <https://doi.org/10.1063/1.5123163> (2019).
- Ding, Z. et al. Quantitative modeling, optimization, and verification of ⁶³Ni-powered betavoltaic cells based on three-dimensional ZnO nanorod arrays. *Nucl. Sci. Techniques* **33**. <https://doi.org/10.1007/s41365-022-01127-6> (2022).
- Sychov, M. et al. Alpha indirect conversion radioisotope power source. *Appl. Radiat. Isotopes* **66**, 173–177 (2008).
- Qiao, D. Y., Chen, X. J., Ren, Y. & Yuan, W. Z. A micro nuclear battery based on SiC Schottky barrier diode. *J. Microelectromech. Syst.* **20**, 685–690 (2011).
- Rybicki, G., Vargas-Aburto, C., & Uribe, R. Silicon carbide alphavoltaic battery. *Conference Record of the IEEE Photovoltaic Specialists Conference*, 93–96. <https://doi.org/10.1109/pvsc.1996.563955> (1996).
- Bormashov, V. et al. Development of nuclear microbattery prototype based on Schottky barrier diamond diodes. *Phys. Status Solidi (A) Appl. Mater. Sci.* **212**, 2539–2547 (2015).
- Liu, L. et al. Silicon carbide PIN diode detectors used in harsh neutron irradiation. *Sens. Actuators A Phys.* **280**, 245–251 (2018).
- Liu, L., et al. Radiation resistance of silicon carbide Schottky diode detectors in D-T fusion neutron detection. *Sci. Rep.* **7**. <https://doi.org/10.1038/s41598-017-13715-3> (2017).
- Cress, C. D., Landi, B. J., Raffaele, R. P., & Wilt, D. M. InGaP alpha voltaic batteries: synthesis, modeling, and radiation tolerance. *J. Appl. Phys.* **100**. <https://doi.org/10.1063/1.2390623> (2006).
- Zheng, R. et al. Understanding efficiency improvements of betavoltaic batteries based on 4H-SiC, GaN, and diamond. *Appl. Phys. Lett.* **121**. <https://doi.org/10.1063/5.0102995> (2022).
- Lioliou, G., Krysa, A. B., & Barnett, A. M. Wide bandgap semiconductor conversion devices for radioisotope microbatteries. *Mater. Sci. Semicond. Process* **142**. <https://doi.org/10.1016/j.mssp.2022.106533> (2022).
- Liu, L., Ouyang, X., Gao, R., Wan, P., & Ouyang, X. Latest developments in room-temperature semiconductor neutron detectors: prospects and challenges. *Sci. China Phys. Mech. Astron.* **66**. <https://doi.org/10.1007/s11433-022-2021-6> (2023).
- Liu, B. et al. Alpha-voltaic battery on diamond Schottky barrier diode. *Diam. Relat. Mater.* **87**, 35–42 (2018).
- Liu, B. et al. Effect of americium-241 source activity on total conversion efficiency of diamond alpha-voltaic battery. *Int. J. Energy Res.* **43**, 6038–6044 (2019).
- Gao, R. et al. High-performance alpha-voltaic cell based on a 4H-SiC PIN junction diode. *Energy Convers. Manag.* **252**, 115090 (2022).
- Xue, J. et al. Silicon substrate diamond film detector for gamma dose rate measurement in a high radiation environment. *Diam. Relat. Mater.* **121**. <https://doi.org/10.1016/j.diamond.2021.108752> (2022).
- Liu, Y. P. et al. Influences of planar source thickness on betavoltaics with different semiconductors. *J. Radioanal. Nucl. Chem.* **304**, 517–525 (2015).
- Liu, B. et al. Enhanced performance of diamond Schottky nuclear batteries by using ZnO as electron transport layer. *Diam. Relat. Mater.* **109**. <https://doi.org/10.1016/j.diamond.2020.108026> (2020).

26. Jabbar, H. D., Fakhri, M. A. & Jalal Abdulrazzaq, M. Gallium nitride -based photodiode: a review. In *Materials Today: Proceedings* (Elsevier Ltd), pp. 2829–2834. <https://doi.org/10.1016/j.matpr.2020.12.729> (2021).
27. Fu, H. et al. Selective area regrowth and doping for vertical gallium nitride power devices: materials challenges and recent progress. *Mater. Today* **49**, 296–323 (2021).
28. Tan, A. K., Hamzah, N. A., Ahmad, M. A., Ng, S. S., & Hassan, Z. Recent advances and challenges in the MOCVD growth of indium gallium nitride: a brief review. *Mater. Sci. Semicond. Process* **143**. <https://doi.org/10.1016/j.mssp.2022.106545> (2022).
29. Wang, J., Mulligan, P., Brillson, L., & Cao, L. R. Review of using gallium nitride for ionizing radiation detection. *Appl. Phys. Rev.* **2**. <https://doi.org/10.1063/1.4929913> (2015).
30. Nord, J., Nordlund, K., Keinonen, J. & Albe, K. Molecular dynamics study of defect formation in GaN cascades. In *Nuclear Instruments and Methods in Physics Research, Section B: Beam Interactions with Materials and Atoms*, pp. 93–99. [https://doi.org/10.1016/S0168-583X\(02\)01839-6](https://doi.org/10.1016/S0168-583X(02)01839-6) (2003).
31. Sandupatla, A. et al. Vertical GaN-on-GaN Schottky diodes as α -particle radiation sensors. *Micromachines (Basel)* **11**. <https://doi.org/10.3390/mi11050519> (2020).
32. Sandupatla, A. et al. Low voltage high-energy α -particle detectors by GaN-on-GaN Schottky diodes with record-high charge collection efficiency. *Sensors (Switzerland)* **19**. <https://doi.org/10.3390/s19235107> (2019).
33. Liu, L. Y., Ouyang, X., Ruan, J. L., Bai, S. & Ouyang, X. P. Performance comparison between SiC and Si neutron detectors in deuterium-tritium fusion neutron irradiation. *IEEE Trans. Nucl. Sci.* **66**, 737–741 (2019).
34. Liu, L. Y., Ouyang, X. P., Zhang, J. F., Jin, P. & Su, C. L. Properties comparison between nanosecond X-ray detectors of polycrystalline and single-crystal diamond. *Diam. Relat. Mater.* **73**, 248–252 (2017).
35. Rebai, M. et al. Pixelated single-crystal diamond detector for fast neutron measurements. *J. Instrum.* **10**. <https://doi.org/10.1088/1748-0221/10/03/C03016> (2015).
36. Lu, M., Wang, G. & Yao, C. Gallium nitride for nuclear batteries. In *Adv. Mater. Res.* pp. 56–61. <https://doi.org/10.4028/www.scientific.net/AMR.343-344.56> (2012).
37. San, H., Yao, S., Wang, X., Cheng, Z. & Chen, X. Design and simulation of GaN based Schottky betavoltaic nuclear micro-battery. *Appl. Radiat. Isotopes* **80**, 17–22 (2013).
38. Lu, M. et al. Gallium nitride schottky betavoltaic nuclear batteries. *Energy Convers. Manag.* **52**, 1955–1958 (2011).
39. Li, F., Gao, X., Yuan, Y., Yuan, J. & Lu, M. GaN PIN betavoltaic nuclear batteries. *Sci China Technol. Sci.* **57**, 25–28 (2014).
40. Hubbard, L. et al. GaN nuclear batteries: radiation modeling for the accelerated contact exposure of betavoltaics. *MRS Adv.* **5**, 1483–1489 (2020).
41. Cheng, Z. J., San, H. S., Feng, Z. H., Liu, B. & Chen, X. Y. High open-circuit voltage betavoltaic cell based on GaN pin homojunction. *Electron Lett.* **47**, 720–722 (2011).
42. Kim, D. S., Yoon, Y. J., Lee, J. S., Kang, I. M. & Lee, J. H. Experimental and simulation study of power performance improvement of GaN PIN betavoltaic cell. *Int. J. Energy Res.* **45**, 17622–17630 (2021).
43. Geng, X. et al. Enhanced energy resolution of GaN-on-sapphire p-i-n alpha-particle detector with isoelectronic Al-doped i-GaN layer. *IEEE Trans. Nucl. Sci.* **68**, 2301–2308 (2021).
44. Lyons, J. L., Janotti, A. & Van De Walle, C. G. Effects of carbon on the electrical and optical properties of InN, GaN, and AlN. *Phys. Rev. B Condens. Matter Mater. Phys.* **89**. <https://doi.org/10.1103/PhysRevB.89.035204> (2014).
45. Seager, C. H., Wright, A. F., Yu, J. & Götz, W. Role of carbon in GaN. *J. Appl. Phys.* **92**, 6553–6560 (2002).
46. Kumakura, K. et al. Minority carrier diffusion length in GaN: dislocation density and doping concentration dependence. *Appl. Phys. Lett.* **86**, 1–3 (2005).
47. Bandić, Z. Z., Bridger, P. M., Piquette, E. C. & McGill, T. C. The values of minority carrier diffusion lengths and lifetimes in GaN and their implications for bipolar devices. *Solid State Electron* **44**, 221–228 (2000).
48. Knoll, G. F. *Radiation Detection and Measurement* 4th ed. (John Wiley & Sons, Inc) (2010).
49. Heinke, H., Kirchner, V., Einfeldt, S. & Hommel, D. X-ray diffraction analysis of the defect structure in epitaxial GaN. *Appl. Phys. Lett.* **77**, 2145–2147 (2000).
50. Yamaguchi, S. et al. Control of strain in GaN using an In doping-induced hardening effect. *Phys. Rev. B Condens. Matter Mater. Phys.* **64**. <https://doi.org/10.1103/PhysRevB.64.035318> (2001).
51. Hikosaka, T., Honda, Y., Yamaguchi, M., and Sawaki, N. Al doping in (1–101) GaN films grown on patterned (001)Si substrate. *J. Appl. Phys.* **101**. <https://doi.org/10.1063/1.2734098> (2007).

Acknowledgements

The work was funded by the National Natural Science Foundation of China (grant numbers 11922507, 12050005, 12075045, 12105033), and the Fundamental Research Funds for the Central Universities (grant number 2021NTST14).

Author contributions

Conceptualization, L.Y.L., H.W.L., and X.P.O.; Methodology, R.L.G., L.Y.L., and X.C.X.; Investigation, R.L.G., P.Y.W., and X.O.; Resources, X.C.X., X.L.G., K.X.Z., and H.W.L.; Data Curation, R.L.G., P.Y.W., W.Y.M., H.Y.W., and R.L.X.; Writing—Original Draft, R.L.G., L.Y.L., and X.C.X.; Writing—Review & Editing, P.Y. Wan, and X.O.

Competing interests

The authors declare no competing interests.

Additional information

Supplementary information The online version contains supplementary material available at <https://doi.org/10.1038/s43246-023-00360-9>.

Correspondence and requests for materials should be addressed to Linyue Liu or Xiaoping Ouyang.

Peer review information *Communications Materials* thanks Dong-Seok Kim and the other, anonymous, reviewer(s) for their contribution to the peer review of this work. Primary Handling Editors: Jet-Sing Lee and John Plummer. Peer reviewer reports are available.

Reprints and permission information is available at <http://www.nature.com/reprints>

Publisher's note Springer Nature remains neutral with regard to jurisdictional claims in published maps and institutional affiliations.



Open Access This article is licensed under a Creative Commons Attribution 4.0 International License, which permits use, sharing, adaptation, distribution and reproduction in any medium or format, as long as you give appropriate credit to the original author(s) and the source, provide a link to the Creative Commons license, and indicate if changes were made. The images or other third party material in this article are included in the article's Creative Commons license, unless indicated otherwise in a credit line to the material. If material is not included in the article's Creative Commons license and your intended use is not permitted by statutory regulation or exceeds the permitted use, you will need to obtain permission directly from the copyright holder. To view a copy of this license, visit <http://creativecommons.org/licenses/by/4.0/>.

© The Author(s) 2023